Available online at www.sciencedirect.com
SCIENCE DIRECT®
Journal of Solid State Chemistry 177 (2004) 2470–2476
JOURNAL OF SOLID STATE CHEMISTRY
http://elsevier.com/locate/jssc

# Preparation and structural study from neutron diffraction data of $R_2MoO_6$ ($R$= Dy, Ho, Er, Tm, Yb, Y)

J.A. Alonso,[a,*] F. Rivillas,[a] M.J. Martínez-Lope,[a] and V. Pomjakushin[b]

[a] *Instituto de Ciencia de Materiales de Madrid, C.S.I.C., Cantoblanco, E-28049 Madrid, Spain*
[b] *Laboratory for Neutron Scattering, ETHZ & PSI, CH-5232 Villigen PSI, Switzerland*

Received 21 January 2004; received in revised form 26 March 2004; accepted 29 March 2004

**Abstract**

The title compounds have been prepared as polycrystalline powders by thermal treatments of stoichiometric mixtures of $R_2O_3$ and $MoO_3$ in air. The room-temperature crystal structure for all the series has been refined from high-resolution neutron powder diffraction data. All the phases are isostructural (space group $C2/c$, $Z = 8$) with the polymorph $\alpha$-$R_2MoO_6$, typified by $Sm_2MoO_6$. The structure contains four zigzag, one-dimensional $MoO_5$ polyhedral rows per unit cell, running through the $RO_8$ polyhedral framework along the [001] direction. $MoO_5$ form discrete units (i.e. do not share common oxygen), with Mo–O distances ranging from 1.77 to 2.24 Å, although the oxygen coordination can be extended to distances of about 3.1 Å, giving rise to strongly distorted $MoO_8$ scalenohedra. Thus, $MoO_8$ and $RO_8$ polyhedra are fully ordered in $R_2MoO_6$ compounds, which in fact can be considered as superstructures of fluorite ($M_3O_6$), containing 24 $MO_2$ fluorite units per unit cell, with unit-cell parameters related to that of cubic fluorite ($\boldsymbol{a}_f = 5.5$ Å). A bond valence study demonstrates that the present crystal structure is especially stable for small rare-earth cations, and becomes more unstable when the $R^{3+}$ size increases, thus explaining the observed preference of the large rare-earth molybdates for polymorphs $\beta$ and $\gamma$ with the same stoichiometry.


*Keywords:* Rare-earth molybdates; Neutron diffraction; Crystal structure; Mo(VI); Bond valence

## 1. Introduction

Complex oxides of composition $R_2MoO_6$ ($R$= rare earths or Bi) are well known for their catalytic properties. For instance, $Bi_2MoO_6$ is an extensively used catalytic component for selective olefin oxidation [1]; $La_2MoO_6$ [2] and $Pr_2MoO_6$ [3,4] have also been described as catalysts in the selective oxidation of toluene and isobutene, respectively. Depending on the size or the synthesis conditions, $R_2MoO_6$ compounds have been described to crystallize in three polymorphs, with monoclinic ($\alpha$), cubic ($\beta$) and tetragonal ($\gamma$) symmetries [5,6]. $La_2MoO_6$ preferentially adopts the tetragonal $\gamma$ form [6,7] under standard solid state conditions, whereas Ce prefers a pseudo-cubic, fluorite-related structure [6–10], the details of which are still unknown. For Pr and Nd, the tetragonal form is the high-temperature phase, whereas the pseudo-cubic structure ($\beta$) can be stabilized at low temperatures [7]. Most of the small-sized rare-earth cations (Sm–Lu and Y) are reported to form the monoclinic ($\alpha$) phase [5,6]. The $\alpha$ polymorph, closely related to the scheelite-type structure, was first described for the tungstate compounds $R_2WO_6$ ($R$=Nd or Gd) [11,12]. This polymorph has been typified for the Sm and Gd molybdate analogues, the crystal structure of which has been described in two different settings of the space group No. 15: $I2/c$ and $C2/c$ [5,12]. The structural relationship between the $\alpha$ phase ($I2/c$ setting) and the monoclinic scheelite structure is given by $a \approx 3a_s \approx 15.5$ Å; $b \approx c_s \approx 11.0$ Å; $c \approx b_s \approx 5.4$ Å; $\beta \approx \beta_s \approx 91°$. Scheelite itself is a superstructure of fluorite ($CaF_2$, cubic, $\boldsymbol{a} = 5.5544$ Å, $Fd\bar{3}m$ [13]). The crystal structure of the $\alpha$ $Tb_2MoO_6$ phase has been refined in the $C2/c$ space group from neutron powder diffraction (NPD) data [7]. It can be described as four zigzag, one-dimensional $MoO_5$ polyhedral rows per unit cell

*Corresponding author. Fax: +34-91-372-0623.
*E-mail address:* ja.alonso@icmm.csic.es (J.A. Alonso).

0022-4596/$ - see front matter © 2004 Elsevier Inc. All rights reserved.
doi:10.1016/j.jssc.2004.03.046

running through the $TbO_8$ polyhedral framework along the [001] direction.

This paper reports on the preparation of polycrystalline samples and crystal structure study of the α-$R_2MoO_6$ polymorphs for small-sized rare earths, $R$ = $Y$, Dy, Ho, Er, Tm, Yb. Given the weak scattering power of oxygen with respect to rare earths or molybdenum atoms, NPD has been the technique of choice for this investigation. The Sm, Eu and Gd compounds were excluded from this study given the high neutron absorption cross-section of these rare earths. The structural evolution and stability across the series is discussed on light of a bond-valence study as a function of the rare-earth cation size.

## 2. Experimental

Polycrystalline $R_2MoO_6$ ($R$ = Dy, Ho, Er, Tm, Yb, Y) samples were prepared by solid-state reaction, from stoichiometric amounts of analytical grade $R_2O_3$ and $MoO_3$. The reactants were mixed, ground and calcined at 1150°C for 12 h in air.

The initial characterization of the products was carried out by laboratory X-ray diffraction (XRD) (Cu$K\alpha$, $\lambda = 1.5406$ Å). NPD diagrams were collected at the high resolution HRPT diffractometer of the SINQ spallation source, at Paul Scherrer Institute, Zurich. The patterns were collected at room temperature with a wavelength of 1.494 Å. The high intensity mode was used; the collection time was 2 h, excepting for the absorbing $Dy_2MoO_6$ sample, collected in 9 h. A 6 mm dia. vanadium can was used; for $Dy_2MoO_6$ a double-walled vanadium sample holder was employed to minimize absorption. The refinement of the crystal structures was performed by the Rietveld method, using the FULLPROF refinement program [14]. A pseudo-Voigt function was chosen to generate the line shape of the diffraction peaks. The following parameters were refined in the final runs: scale factor, background coefficients, zero-point error, pseudo-Voigt corrected for asymmetry parameters, positional coordinates and isotropic thermal factors. The absorption of the $R_2MoO_6$ samples was measured and $\mu R$ values of 0.674, 0.193, 0.308, 0.193 and 0.099 for $R$ = Dy, Ho, Er, Tm and Yb, respectively, were considered during the refinement. The coherent scattering lengths for Dy, Ho, Er, Tm, Yb, Y, Mo and O were 16.9, 8.01, 7.79, 7.07, 12.4, 7.75, 6.72 and 5.803 fm, respectively.

## 3. Results and discussion

$R_2MoO_6$ oxides were obtained as polycrystalline, pale colored materials (white for Y, Dy, Tm and Yb; yellow for Ho and pink for Er). Fig. 1 shows the XRD patterns

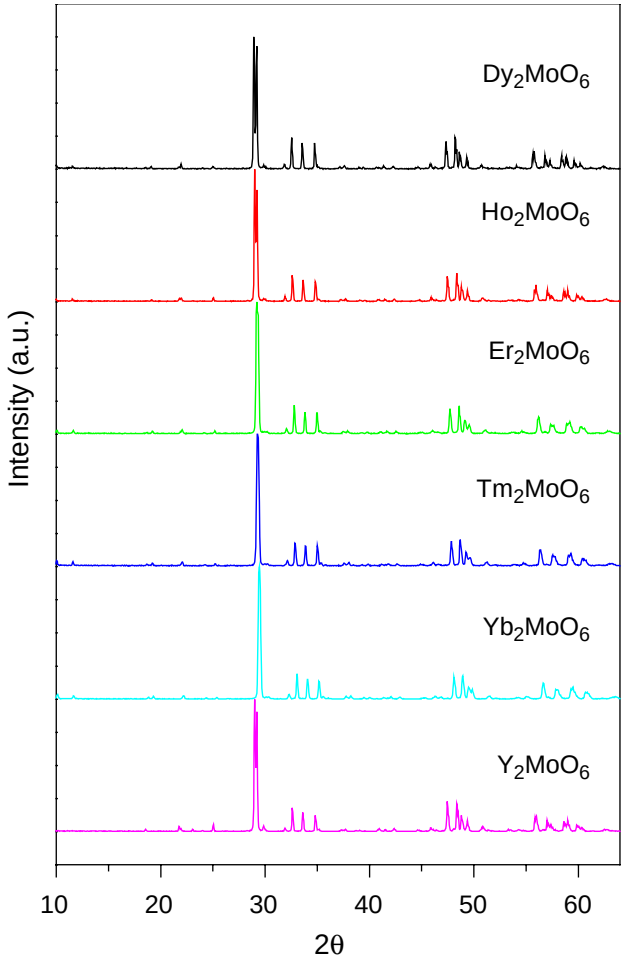


Fig. 1. XRD patterns of $R_2MoO_6$ ($R$ = Dy, Ho, Er, Tm, Yb and Y) prepared by solid-state reaction of $R_2O_3$ and $MoO_3$ in air.

of $R_2MoO_6$ ($R$= Dy, Ho, Er, Tm, Yb, Y). They all correspond to pure phases, that can be indexed in a monoclinic unit cell, isotypic to $Gd_2MoO_6$ (International Center for Diffraction Data, PDF file 78-1203). Fig. 2 illustrates the indexing of the XRD reflections of $Dy_2MoO_6$. The corresponding PDF files for Dy, Ho, Er and Tm have been published (Nos. 24-0388, 25-0376, 25-0332 and 25-0972, respectively). The unit-cell parameters the Y and Yb compounds were reported by Brixner et al. [6]. To complement the existing X-ray powder diffraction files, in Tables 1 and 2 we include the diffraction data corresponding to the materials with $R$ = $Y$, Yb.

The crystal structures were refined from RT high-resolution NPD data in both the $C2/c$ and $I2/c$ settings of the space group No. 15, $Z = 8$, taking as starting models those described for $Tb_2MoO_6$ [7] or $Sm_2MoO_6$ [5], respectively. In both cases we reached exactly the same discrepancy $R$-factors; however the description in $C2/c$ was preferred since it corresponds to the standard space group in the International Tables for Crystallography [15]. We will refer hereafter to the results

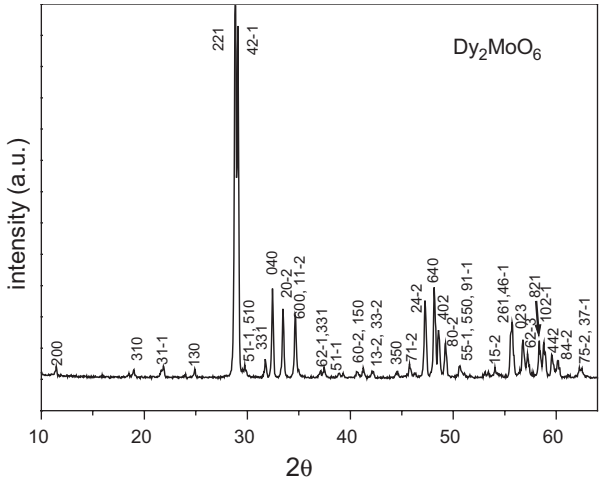


Fig. 2. XRD pattern of $Dy_2MoO_6$, indexed in a monoclinic unit cell with $\boldsymbol{a} = 16.4160(5)$, $\boldsymbol{b} = 11.0745(4)$, $\boldsymbol{c} = 5.3734(2)$ Å, $\beta = 108.385(2)^\circ$.

obtained in the $C2/c$ setting. In the asymmetric unit there are three independent rare-earth atoms; $R1$ and $R2$ at $4e$ $(0, y, \frac{1}{4})$ positions, and $R3$ at general $8f$ $(x, y, z)$ sites. Mo and O1, O2, O3, O4, O5 and O6 are also placed at $8f$ positions. Fig. 3 illustrates the goodness of the NPD fit for $Dy_2MoO_6$. The refined unit-cell parameters and volumes for the different compounds of the $R_2MoO_6$ series are listed in Table 3. They show a regular variation with the ionic radii of the rare-earth cations [16], according to the well-known lanthanide contraction, as displayed in Fig. 4. The actual ionic radius for $Y^{3+}$ seems to be smaller in this structure than that given in the literature for eight-fold coordination [16]. The final atomic coordinates and isotropic thermal factors after the refinement are listed in Table 4. Final bonding distances are given in Table 5.

The overall structural features correspond to those described for $Tb_2MoO_6$ [7]. A representation of the structure is shown in Fig. 5. Mo is coordinated to five oxygen atoms at distances between 1.76 and 2.24 Å conforming strongly distorted trigonal bi-pyramidal $MoO_5$ units. These units form bilayers perpendicular to the $\boldsymbol{a}$-axis, separated apart by $RO_8$ polyhedra, as shown in Fig. 5. In fact, there are three additional longer Mo–O distances between 2.93 and 3.11 Å which could also be considered to take part of the Mo environment, in a very distorted $MoO_8$ scalenohedron, as illustrated in Fig. 6. Actually, the bond valences corresponding to these long Mo–O bonds are smaller than 0.1 valence units, in such a way that they may be neglected. The $MoO_5$ bi-pyramidal polyhedra are isolated (they do not share common oxygens), forming discrete units. This may supply structural grounds for the insulating behavior observed in most of the $R_2MoO_6$ compounds. The three kinds of oxygen environment for rare earth cations can also be defined as rather distorted scalenohedra. For instance, for $Dy_2MoO_6$, the $R1O_8$ polyhedron contains $R1$–O bond lengths ranging between 2.24 and 2.75 Å, with average $\langle R1-O \rangle$ distances of 2.42 Å; in $R2O_8$ the distances range from 2.20 to 2.47 Å, with a $\langle R2-O \rangle$ average of 2.38 Å, and $R3O_8$ units show distances between 2.17 and 2.63 Å, with $\langle R3-O \rangle$ of 2.40 Å.

Table 1
X-ray powder diffraction data for $Y_2MoO_6$

| $d$ (Å) | $I/I_0$ | $h\,k\,l$ |
|---|---|---|
| 4.848 | 1 | 1 1 −1 |
| 4.124 | 3 | 1 1 1 |
| 4.095 | 2 | 3 1 −1 |
| 3.900 | 1 | 4 0 0 |
| 3.590 | 4 | 1 3 0 |
| 3.105 | 100 | 2 2 1 |
| 3.084 | 78 | 4 2 −1 |
| 3.018 | 4 | 5 1 −1 |
| 2.823 | 2 | 3 3 −1 |
| 2.763 | 15 | 0 4 0 |
| 2.687 | 12 | 2 0 −2 |
| 2.592 | 12 | 6 0 0 |
| 2.571 | 2 | 1 1 −2 |
| 2.426 | 1 | 4 2 1 |
| 2.401 | 1 | 3 3 1 |
| 2.222 | 1 | 2 4 1 |
| 2.217 | 2 | 4 4 −1 |
| 2.189 | 1 | 1 5 0 |
| 2.144 | 2 | 3 3 −2 |
| 2.040 | 1 | 6 2 −2, 3 5 0 |
| 1.987 | 2 | 7 1 −2 |
| 1.965 | 1 | 1 5 1, 7 3 −1 |
| 1.924 | 20 | 2 4 −2 |
| 1.890 | 22 | 6 4 0 |
| 1.873 | 11 | 4 0 2 |
| 1.854 | 7 | 8 0 −2 |
| 1.804 | 3 | 5 5 −1 |
| 1.786 | 1 | 5 5 0, 9 1 −1 |
| 1.725 | 1 | 1 1 −3 |
| 1.695 | 1 | 1 5 −2 |
| 1.652 | 10 | 2 6 1 |
| 1.648 | 11 | 4 6 −1 |
| 1.620 | 7 | 0 2 3 |
| 1.610 | 5 | 6 2 −3 |
| 1.579 | 7 | 8 2 1 |
| 1.570 | 7 | 10 2 −1 |
| 1.549 | 4 | 4 4 2, 9 3 −2 |
| 1.545 | 3 | 8 4 −2 |
| 1.490 | 1 | 7 5 −2 |
| 1.486 | 1 | 3 7 −1 |
| 1.380 | 1 | 0 8 0 |
| 1.352 | 1 | 1 5 −3 |
| 1.339 | 1 | 3 7 −2 |

If we consider, for descriptive purposes, the occurrence of strongly distorted $MoO_8$ scalenohedra together with $RO_8$ polyhedral units, it is simple to understand the relationship of this complex superstructure with the basic fluorite $CaF_2$ structure, containing regular $CaF_8$ units in a cubic coordination. The $\boldsymbol{a}$, $\boldsymbol{b}$ and $\boldsymbol{c}$ unit-cell parameters of the monoclinic structure of $R_2MoO_6$ are related with the simple cubic fluorite unit cell (with

Table 2
X-ray powder diffraction data for $Yb_2MoO_6$

| $d$ (Å) | $I/I_0$ | $h\,k\,l$ |
|---|---|---|
| 8.822 | 6 | 1 1 0 |
| 7.611 | 2 | 2 0 0 |
| 4.727 | 1 | 1 1 −1 |
| 4.610 | 2 | 3 1 0 |
| 4.026 | 2 | 3 1 −1 |
| 3.523 | 1 | 1 3 0 |
| 3.045 | 100 | 2 2 1, 4 2 −1 |
| 2.956 | 2 | 5 1 0, 5 1 −1 |
| 2.779 | 3 | 3 3 −1 |
| 2.713 | 16 | 0 4 0 |
| 2.635 | 11 | 2 0 −2 |
| 2.557 | 14 | 6 0 0 |
| 2.527 | 2 | 1 1 −2 |
| 2.389 | 2 | 4 2 1 |
| 2.363 | 2 | 3 3 1 |
| 2.286 | 1 | 5 1 −2 |
| 2.257 | 1 | 5 1 1 |
| 2.186 | 1 | 2 4 1 |
| 2.154 | 1 | 1 5 0, 6 0 −2 |
| 2.113 | 1 | 3 3 −2 |
| 2.004 | 1 | 3 5 0 |
| 1.961 | 2 | 7 1 −2 |
| 1.941 | 1 | 7 3 −1 |
| 1.894 | 15 | 2 4 −2 |
| 1.864 | 17 | 6 4 0 |
| 1.843 | 9 | 4 0 2 |
| 1.833 | 6 | 8 0 −2 |
| 1.776 | 2 | 5 5 −1 |
| 1.692 | 1 | 5 5 0 |
| 1.665 | 2 | 1 5 −2 |
| 1.626 | 11 | 2 6 1, 4 6 −1 |
| 1.614 | 1 | 9 3 −1 |
| 1.595 | 7 | 0 2 3 |
| 1.591 | 6 | 6 2 −3 |
| 1.558 | 7 | 8 2 1 |
| 1.556 | 8 | 5 3 −3, 10 2 −1 |
| 1.526 | 4 | 4 4 2, 8 4 −2 |
| 1.470 | 1 | 7 5 −2 |
| 1.464 | 1 | 3 7 −1 |
| 1.360 | 1 | 0 8 0 |
| 1.349 | 1 | 3 7 −2 |

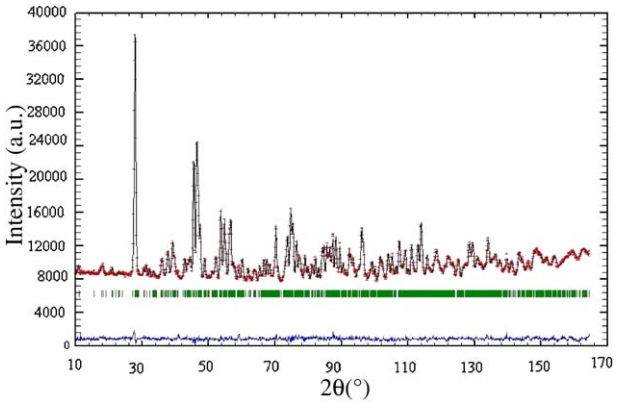


Fig. 3. Observed (crosses), calculated (solid line) and difference (at the bottom) NPD for $Dy_2MoO_6$ at 295 K. The tick marks indicate the positions of the allowed Bragg reflections.

Table 3
Unit-cell parameters and volume for $R_2MoO_6$ determined from NPD at room temperature

| $R$ | $r(R^{3+})$ (Å)[a] | $a$ (Å) | $b$ (Å) | $c$ (Å) | $V$ (Å$^3$) | $\beta$ (°) |
|---|---|---|---|---|---|---|
| Dy | 1.027 | 16.4160(5) | 11.0745(4) | 5.3734(2) | 927.01(5) | 108.385(2) |
| Ho | 1.015 | 16.3611(4) | 11.0278(3) | 5.3496(1) | 915.42(4) | 108.486(2) |
| Er | 1.004 | 16.3249(5) | 10.9856(3) | 5.3307(2) | 905.97(5) | 108.617(2) |
| Tm | 0.994 | 16.2809(5) | 10.9382(3) | 5.3120(2) | 896.28(5) | 108.654(2) |
| Yb | 0.985 | 16.2437(4) | 10.8992(3) | 5.2907(1) | 887.50(4) | 108.649(1) |
| Y | 1.019 | 16.3538(4) | 11.0183(3) | 5.3506(1) | 914.19(4) | 108.523(1) |

[a] In eight-fold coordination, taken from Ref. [16].

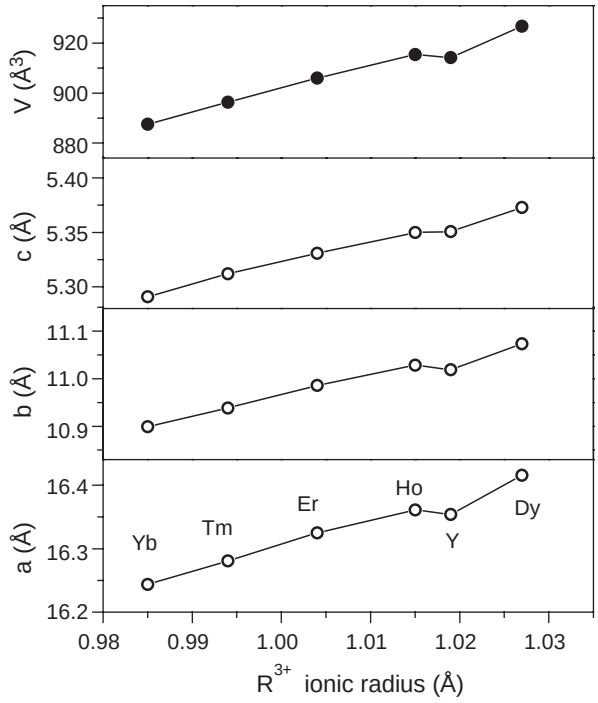


Fig 4. Unit-cell parameters and volume variation with the ionic radii of $R^{3+}$ cations.

orthogonal unit-cell parameter vectors $\boldsymbol{a}_f$, $\boldsymbol{b}_f$ and $\boldsymbol{c}_f$ of equal modulus of 5.5 Å) as $\boldsymbol{a} \approx 3\boldsymbol{a}_f + \boldsymbol{c}_f$, $\boldsymbol{b} \approx 2\boldsymbol{b}_f$ and $\boldsymbol{c} \approx \boldsymbol{c}_f$, with a $\beta$ angle between $\boldsymbol{a}$ and $\boldsymbol{c}$ close to 108°. $R_2MoO_6$ can be rewritten as $M_3O_6$, containing 3 fluorite $MO_2$ units per formula and 24 $MO_2$ units per unit cell. The complex monoclinic superstructure thus results from the long range ordering between $RO_8$ and $MoO_8$ polyhedra across the crystal.

The valence of the cations and anions present in the solid can be estimated by means of the Brown's bond valence model [17,18], which gives a phenomenological relationship between the formal valence of a bond and the corresponding bond length. In perfect nonstrained structures the bond valence sum (BVS) rule states that the formal charge of the cation (anion) is equal to the sum of the bond valences around this cation (anion). This rule is satisfied only if the stress introduced by the

Table 4
Structural parameters after the Rielveld refinement of NPD data for $R_2MoO_6$ oxides at room temperature

| Atom | | Dy | Ho | Er | Tm | Yb | Y |
|---|---|---|---|---|---|---|---|
| *R*1 | *y* | 0.3910(3) | 0.3925(3) | 0.3936(4) | 0.3932(3) | 0.3933(2) | 0.3929(3) |
| *B* (Å$^2$) | | −0.04(5) | 0.25(6) | 0.28(7) | 0.52(7) | 0.28(4) | 0.39(5) |
| *R*2 | *y* | 0.8644(3) | 0.8640(3) | 0.8635(4) | 0.8631(4) | 0.8631(2) | 0.8644(3) |
| *B* (Å$^2$) | | 0.24(5) | 0.29(6) | 0.55(7) | 0.58(7) | 0.48(4) | 0.51(5) |
| *R*3 | *x* | 0.3318(1) | 0.3318(2) | 0.3320(2) | 0.3329(2) | 0.3332(1) | 0.3316(1) |
| | *y* | 0.1174(2) | 0.1174(2) | 0.1171(3) | 0.1166(3) | 0.1167(2) | 0.1167(2) |
| | *z* | 0.1182(4) | 0.1208(4) | 0.1198(5) | 0.1204(5) | 0.1209(3) | 0.1207(4) |
| *B* (Å$^2$) | | 0.16(4) | 0.37(4) | 0.56(5) | 0.29(5) | 0.36(3) | 0.45(4) |
| Mo | *x* | 0.1540(3) | 0.1546(2) | 0.1552(2) | 0.1551(2) | 0.1552(2) | 0.1545(2) |
| | *y* | 0.1408(4) | 0.1414(2) | 0.1402(3) | 0.1402(3) | 0.1401(3) | 0.1418(2) |
| | *z* | 0.442(1) | 0.4400(6) | 0.4388(7) | 0.4391(6) | 0.4398(6) | 0.4405(5) |
| *B* (Å$^2$) | | 0.14(7) | 0.29(5) | 0.46(5) | 0.28(5) | 0.32(5) | 0.22(4) |
| O1 | *x* | 0.2353(4) | 0.2353(2) | 0.2349(3) | 0.2364(2) | 0.2361(3) | 0.2350(2) |
| | *y* | 0.0527(5) | 0.0523(3) | 0.0512(3) | 0.0497(3) | 0.0491(3) | 0.0518(3) |
| | *z* | 0.367(1) | 0.3661(8) | 0.3635(9) | 0.3674(7) | 0.3665(8) | 0.3672(6) |
| *B* (Å$^2$) | | 0.39(9) | 0.87(6) | 0.89(6) | 0.61(5) | 0.80(6) | 0.72(5) |
| O2 | *x* | 0.0791(4) | 0.0797(2) | 0.0797(2) | 0.0791(2) | 0.0789(2) | 0.07917(2) |
| | *y* | 0.0343(5) | 0.0326(3) | 0.0328(3) | 0.0321(3) | 0.0318(3) | 0.0328(2) |
| | *z* | 0.486(1) | 0.4865(6) | 0.4850(7) | 0.4868(6) | 0.4879(7) | 0.4859(5) |
| *B* (Å$^2$) | | 0.41(9) | 0.81(6) | 0.62(6) | 0.59(6) | 0.62(6) | 0.59(5) |
| O3 | *x* | 0.2276(4) | 0.2283(2) | 0.2281(3) | 0.2282(2) | 0.2276(2) | 0.2281(2) |
| | *y* | 0.2011(5) | 0.2034(3) | 0.2042(3) | 0.2044(3) | 0.2043(3) | 0.2038(2) |
| | *z* | 0.738(1) | 0.7402(7) | 0.7425(9) | 0.7443(7) | 0.7453(7) | 0.7408(6) |
| *B* (Å$^2$) | | 0.57(9) | 0.87(5) | 1.00(6) | 0.69(5) | 0.62(6) | 0.68(4) |
| O4 | *x* | 0.1060(4) | 0.1061(3) | 0.1061(3) | 0.1055(2) | 0.1060(3) | 0.1060(2) |
| | *y* | 0.2223(5) | 0.2213(3) | 0.2210(4) | 0.2203(3) | 0.2206(4) | 0.2210(3) |
| | *z* | 0.135(1) | 0.1351(7) | 0.1319(8) | 0.1295(7) | 0.1287(8) | 0.1339(6) |
| *B* (Å$^2$) | | 0.14(9) | 0.94(6) | 0.73(7) | 0.65(6) | 0.91(7) | 0.64(5) |
| O5 | *x* | 0.0725(4) | 0.0719(2) | 0.0716(2) | 0.0705(2) | 0.0703(2) | 0.0718(2) |
| | *y* | 0.2631(5) | 0.2643(3) | 0.2652(3) | 0.2652(3) | 0.2651(3) | 0.2646(2) |
| | *z* | 0.586(1) | 0.5835(8) | 0.5838(8) | 0.5813(7) | 0.5825(8) | 0.5835(6) |
| *B* (Å$^2$) | | 0.40(8) | 0.62(5) | 0.59(5) | 0.65(4) | 0.518(5) | 0.43(4) |
| O6 | *x* | 0.5919(4) | 0.5921(3) | 0.5918(3) | 0.5919(2) | 0.5918(2) | 0.5921(2) |
| | *y* | 0.0180(5) | 0.0181(3) | 0.0197(3) | 0.0189(3) | 0.0192(3) | 0.0183(2) |
| | *z* | 0.578(1) | 0.5781(8) | 0.5795(8) | 0.5787(7) | 0.5797(7) | 0.5791(6) |
| *B* (Å$^2$) | | 0.58(1) | 0.53(5) | 0.49(6) | 0.36(5) | 0.31(5) | 0.31(4) |
| $\chi^2$ | | 2.42 | 3.51 | 1.83 | 2.43 | 2.76 | 2.57 |
| $R_p$ | | 1.20 | 1.64 | 1.86 | 1.72 | 1.96 | 2.34 |
| $R_{wp}$ | | 1.53 | 2.19 | 2.36 | 2.29 | 2.47 | 3.08 |
| $R_{exp}$ | | 0.98 | 1.17 | 1.74 | 1.47 | 1.49 | 1.92 |
| $R_I$ (%) | | 3.16 | 2.72 | 2.50 | 2.51 | 2.03 | 2.09 |

*R*1 and *R*2 at 4*e* $(0,\ y,\ \frac{1}{4})$; *R*3, Mo, O1, O2, O3, O4, O5 and O6 at 8*f* $(x, y, z)$ positions.

coexistence of different structural units can be relieved by the existence of enough degrees of freedom in the crystallographic structure. The departure of the BVS rule is a measure of the existing stress in the bonds of the structure.

Table 6 lists the valences calculated for *R*, Mo and O from the individual *R*−O and Mo–O distances of Table 5 for $R_2MoO_6$. The valences for *R*= Sm and Tb have been calculated from the structural data published in Refs. [5,7]. The valences of the *R* cations are slightly higher than the expected value of +3; in compensation, the valence of Mo atoms is slightly lower than +6. This result suggests that *R* atoms are overbonded while Mo are underbonded in this structure; in other words *R*−O bonds are, in average, under compressive stress and Mo–O bonds are under tensile stress, giving rise to a structure with a slight metastable character.

In Table 5 we can observe that the average $\langle R-O \rangle$ bond lengths decrease from Dy to Yb, as expected for the lanthanide contraction ($Y^{3+}$ is similar to $Ho^{3+}$ in ionic radius). This trend scales with the observed contraction of the unit-cell parameters. However, the average $\langle Mo-O \rangle$ distances (considering only the 5 short bonds) does not significantly change across the series. Consistently, in $Tb_2MoO_6$, the average $\langle Mo-O \rangle$ bond length is 1.885 Å [7]. Therefore, in Table 6 there is no significant variation of the Mo valence from Tb to Yb, within the standard deviations, in spite of the progressive contraction of the unit-cell volume. This fact can be understood taking into account the contribution of covalent bonding to the strength of Mo–O bonds: *R* and Mo cations compete with each other for the electron cloud of $O^{2-}$ through their Coulombic potential $Ze^2/r$ (*Z*: valence, *r*: ionic radius); a $R^{3+}$ cation with a lower Coulombic potential ($Dy^{3+}$ vs $Yb^{3+}$) allows to increase the overlap of the electron clouds between Mo and O ions, giving rise to a stronger Mo–O covalent bonding in $Dy_2MoO_6$: the expected reduction in covalent character for Mo–O bonds across the series is approximately cancelled by the contraction of the lattice due to sterical factors. An even more dramatic trend has been observed in other oxides containing rare-earths and a transition metal in a high oxidation state, such as the $RNiO_3$ perovskites [19], in which Ni–O bond lengths slightly increase from $LaNiO_3$ to $SmNiO_3$ in spite of the significant decrease observed in the cell volume as *R* becomes smaller.

The presence of structural stresses in the crystal structure can be quantified by means of the "Global Instability Index" [20], GII in Table 6, calculated as the root mean of the valence deviations for the $j = 1, \ldots, N$ atoms in the asymmetric unit, according to $GII = (\sum_j[\sum_i(s_{ij} - V_j)^2]/N)^{1/2}$ It is a measure of the extent to which the BVS rule is violated over the whole structure. As suggested by Brown [20] and Armbruster et al. [21], GII values higher than 0.2 v.u. indicate the presence of intrinsic strains large enough to cause instability at room temperature. We observe minimum GII values for Y, Er and Yb, and a noticeable increase from Dy to Sm, reaching the limiting GII factor of 0.2 v.u. The size of the smallest rare-earth cations seems to be adequate to introduce a minimum of stresses into the crystal structure of this series of materials, the instability of which increases with the rare-earth size. In fact, the Sm

Table 5
Selected interatomic distances (Å) in $R_2MoO_6$

| | | Dy | Ho | Er | Tm | Yb | Y |
|---|---|---|---|---|---|---|---|
| R1–O4 | (×2) | 2.753(7) | 2.762(5) | 2.773 (5) | 2.764(5) | 2.762(5) | 2.769(4) |
| –O5 | (×2) | 2.307(7) | 2.287(4) | 2.279(5) | 2.255(4) | 2.251(4) | 2.287(4) |
| –O6 | (×2) | 2.242(7) | 2.229(4) | 2.203(5) | 2.205(4) | 2.192(4) | 2.222(3) |
| –O6 | (×2) | 2.383(7) | 2.365(4) | 2.360(5) | 2.347(4) | 2.342(4) | 2.365(3) |
| ⟨*R*1–O⟩[a] | | 2.421 | 2.411 | 2.404 | 2.393 | 2.387 | 2.411 |
| *R*2–O2 | (×2) | 2.475(6) | 2.481(4) | 2.482(4) | 2.466(4) | 2.452(4) | 2.480(3) |
| –O2 | (×2) | 2.406(6) | 2.390(4) | 2.383(5) | 2.372(5) | 2.362(4) | 2.385(4) |
| –O4 | (×2) | 2.440(6) | 2.423(4) | 2.399(5) | 2.373(4) | 2.368(4) | 2.418(3) |
| –O5 | (×2) | 2.203(7) | 2.202(5) | 2.194(5) | 2.178(4) | 2.165(4) | 2.204(4) |
| ⟨*R*2–O⟩ | | 2.381 | 2.376 | 2.365 | 2.347 | 2.337 | 2.372 |
| *R*3–O1 | | 2.482(7) | 2.459(5) | 2.457(6) | 2.458(5) | 2.456(4) | 2.465(4) |
| –O1 | | 2.555(6) | 2.547(4) | 2.533(5) | 2.497(4) | 2.492(4) | 2.535(4) |
| –O3 | | 2.399(7) | 2.393(4) | 2.379(5) | 2.375(5) | 2.371(4) | 2.394(4) |
| –O3 | | 2.463(7) | 2.427(4) | 2.410(5) | 2.408(5) | 2.394(4) | 2.424(4) |
| –O4 | | 2.630(7) | 2.637(5) | 2.618(5) | 2.608(5) | 2.588(5) | 2.641(4) |
| –O5 | | 2.275(7) | 2.259(4) | 2.249(5) | 2.250(4) | 2.237(4) | 2.263(4) |
| –O6 | | 2.172(7) | 2.174(5) | 2.160(5) | 2.142(5) | 2.137(4) | 2.172(4) |
| –O6 | | 2.279(7) | 2.260(4) | 2.259(5) | 2.237(4) | 2.226(4) | 2.253(4) |
| ⟨*R*3–O⟩ | | 2.401 | 2.395 | 2.383 | 2.372 | 2.363 | 2.393 |
| Mo–O1 | | 1.796(8) | 1.788(5) | 1.773(6) | 1.789(5) | 1.784(5) | 1.788(4) |
| –O1 | | 3.111(8) | 3.097(5) | 3.060(5) | 3.053(5) | 3.029(5) | 3.096(4) |
| –O2 | | 1.774(8) | 1.787(5) | 1.779(5) | 1.788(5) | 1.788(5) | 1.786(4) |
| –O2 | | 3.063(7) | 3.030(4) | 3.013(5) | 2.993(4) | 2.978(5) | 3.037(4) |
| –O3 | | 1.796(8) | 1.809(5) | 1.817(6) | 1.817(5) | 1.808(5) | 1.808(4) |
| –O3 | | 2.995(8) | 2.951(5) | 2.944(6) | 2.938(5) | 2.941(5) | 2.950(4) |
| –O4 | | 1.828(7) | 1.802(5) | 1.808(5) | 1.809(5) | 1.810(5) | 1.804(4) |
| –O5 | | 2.209(8) | 2.217(5) | 2.239(5) | 2.236(5) | 2.235(5) | 2.215(4) |
| ⟨Mo–O⟩$_{(5\ short)}$ | | 1.881 | 1.881 | 1.883 | 1.888 | 1.885 | 1.880 |

[a] ⟨ ⟩ denotes average distance values.

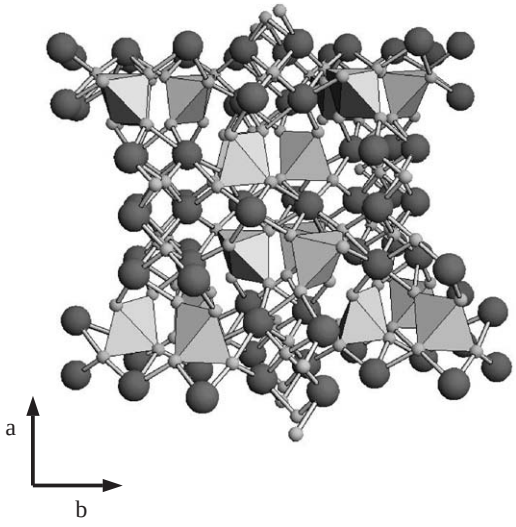


Fig. 5. View of the $R_2MoO_6$ structure in an **ab** projection; $MoO_5$ pyramidal units are connected by $RO_8$ scalenohedra via common oxygen. Small, light spheres represent oxygen; large dark spheres are *R* atoms.

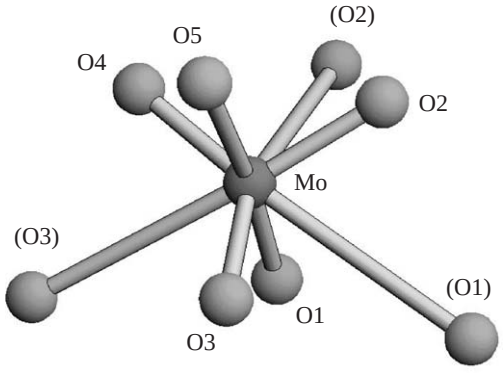


Fig. 6. View of the $MoO_8$ coordination polyhedron: the three oxygen atoms bonded to Mo with long distances (between 2.9 and 3.1 Å) are indicated between parenthesis. Excluding these three oxygen, the $MoO_5$ coordination polyhedron can be described as trigonal bipyramidal units.

compound is the former of the $R_2MoO_6$ series adopting the α structural type. This fact accounts for the stabilization of polymorphs β and γ for $R^{3+}$ ionic radii larger than that of $Sm^{3+}$, as observed in $R_2MoO_6$ ($R$ = La, Ce, Pr, Nd) under standard synthetic solid-state conditions [7].

Table 6
Valences determined from the bond valence model[a] for $R$, Mo and O

| | Sm | Tb | Dy | Ho | Er | Tm | Yb | Y |
|---|---|---|---|---|---|---|---|---|
| R1 | 3.4(1) | 3.27(1) | 3.18(2) | 3.19(1) | 3.19(2) | 2.94(1) | 3.13(1) | 3.13(1) |
| R2 | 3.0(1) | 3.27(1) | 3.29(2) | 3.23(1) | 3.20(2) | 3.27(1) | 3.23(1) | 3.17(1) |
| R3 | 3.2(1) | 3.20(1) | 3.17(2) | 3.17(1) | 3.14(2) | 3.16(2) | 3.10(1) | 3.10(1) |
| Mo | 6.1(4) | 5.75(3) | 5.82(6) | 5.83(4) | 5.84(4) | 5.75(3) | 5.79(4) | 5.83(3) |
| O1 | 2.2(1) | 1.86(2) | 1.90(3) | 1.93(2) | 1.98(2) | 1.93(2) | 1.93(2) | 1.92(2) |
| O2 | 2.1(1) | 2.09(2) | 2.11(3) | 2.04(2) | 2.06(2) | 2.03(2) | 2.02(2) | 2.04(2) |
| O3 | 2.0(1) | 1.99(2) | 2.04(3) | 2.01(2) | 1.98(2) | 1.97(2) | 1.99(2) | 1.99(2) |
| O4 | 1.9(1) | 1.98(2) | 1.92(3) | 1.99(2) | 1.98(2) | 1.86(2) | 1.97(2) | 1.97(1) |
| O5 | 2.2(2) | 2.10(1) | 2.09(2) | 2.07(1) | 2.02(1) | 2.04(1) | 2.02(1) | 2.02(1) |
| O6 | 2.1(2) | 2.21(1) | 2.18(2) | 2.16(1) | 2.16(2) | 2.18(1) | 2.14(1) | 2.13(1) |
| GII | 0.199 | 0.182 | 0.157 | 0.137 | 0.123 | 0.149 | 0.122 | 0.106 |

The valences for Sm and Tb compounds are calculated from the structural data given in Refs. [5,7].

[a] The valence is the sum of the individual bond valences ($s_i$) for $R$–O and Mo–O bonds. Bond valences are calculated as $s_i = \exp[(r_0 - r_i)/B]$; $B = 0.37$, $r_0 = 1.907$ for the $Mo^{6+}$–$O^{2-}$ pair; for the $R^{3+}$–$O^{2-}$ pairs, from Sm to Y, $r_0 = 2.088$, 2.049, 2.036, 2.023, 2.010, 2.000, 1.985, 2.014, from Ref. [18]. Individual $R$–O and Mo–O distances ($r_i$) are taken from Table 5. The global instability index (GII) is calculated as the root mean of the valence deviations for the $j = 1, \ldots, N$ atoms in the asymmetric unit, according to $GII = (\sum_j [\sum_i (s_{ij} - V_j)^2]/N)^{1/2}$.

## 4. Conclusions

The $\alpha - R_2MoO_6$ polymorph has been investigated for rare-earth cations with ionic sizes from 1.027 ($Dy^{3+}$) to 0.985 ($Yb^{3+}$). The crystal structure, refined from NPD data, contains three types of distorted $RO_8$ scalenohedra, which alternate with $MoO_5$ pyramids in a six-fold superstructure of fluorite. Whereas the size of $RO_8$ units scales with the unit-cell volume, the $Mo^{6+}O_5$ bi-pyramidal units tend to maintain the same size from Tb [7] and Dy to the Yb phase, in spite of the contraction observed in the unit-cell parameters and volume as $R$ becomes smaller. This effect can be correlated with the ability of the more basic rare earths to favor the formation of short, covalent Mo–O bonds for the compounds containing larger rare earths. The Global Instability Index, being a measure of the extent to which the BVS rule is violated over the whole structure, noticeably increases for the large rare earths, thus accounting for the trend observed for La, Ce, Pr and Nd to stabilize different molybdate polymorphs ($\beta$ and $\gamma$) with the same stoichiometry.

## Acknowledgments

The authors acknowledge the financial support of the MCyT to the Project MAT2001-0539. This work was partially performed at the spallation source SINQ, Paul Scherrer Institute, Villigen, Switzerland.

## References

[1] D.J. Buttrey, T. Vogt, U. Wildgruber, W.R. Robinson, J. Solid State Chem. 111 (1994) 118.
[2] D.D. Agarwal, K.L. Madhok, H.S. Goswami, React. Kinet. Catal. Lett. 2 (1994) 225.
[3] F. De Smet, M. Devillers, C. Poleunis, P. Bertrand, J. Chem. Soc. Faraday Trans. 94 (1998) 941.
[4] F. De Smet, P. Ruiz, B. Delmon, M. Devillers, J. Phys. Chem. B 105 (2001) 12355.
[5] P.V. Klevtsov, L.Y. Kharchenko, R.F. Kleftsova, Sov. Phys. Crystallogr. 20 (1975) 349.
[6] L.H. Brixner, A.W. Sleigh, M.S. Licis, J. Solid State Chem. 5 (1972) 186.
[7] J.S. Xue, M.R. Antonio, L. Soderholm, Chem. Mater. 7 (1995) 333.
[8] P. Manthiram, J. Golapakrishnan, J. Less Comm. Met. 99 (1984) 107.
[9] M.R. Antonio, J.S. Xue, L. Soderholm, J. Alloys Compounds 207 (1994) 444.
[10] M.R. Antonio, U. Staub, J.S. Xue, L. Soderholm, Chem. Mater. 8 (1996) 2673.
[11] A.V. Tyulin, V.A. Efremov, Sov. Phys. Crystallogr. 32 (1987) 215.
[12] T.M. Polyanskaya, S.V. Borisov, N.V. Belov, Sov. Phys. Crystallogr. 15 (1971) 636.
[13] L.H. Brixner, Rev. Chim. Mineral 10 (1973) 47.
[14] J. Rodríguez-Carvajal, Physica B 192 (1993) 55.
[15] International Tables for Crystallography, Vol. A "Space Group Symmetry", D. Reidel Publ. Comp., Dordrecht, 1983.
[16] R.D. Shannon, Acta Crystallogr. A 32 (1976) 751.
[17] I.D. Brown, in: M. O'Keefe, A. Navrotsky (Eds.), Structure and Bonding in Crystals, Vol. 2, New York: Academic Press, 1981, p. 1.
[18] N.E. Brese, M. O'Keefe, Acta Crystallogr. B 47 (1991) 192.
[19] J.A. Alonso, M.J. Martínez-Lope, I. Rasines, J. Solid State Chem. 120 (1995) 170.
[20] I.D. Brown, Z. Kristallogr. 199 (1992) 255.
[21] T. Armbuster, F. Röthlisberger, F. Seifer, Am. Mineral 75 (1990) 847.